

1 **Solar forced diurnal regulation of cave drip rates via phreatophyte evapotranspiration**

2

3 Katie Coleborn^{1,4}, Gabriel C. Rau^{1,2}, Mark O. Cuthbert³, Andy Baker^{1,4}, Owen Navarre⁴

4 ¹*Connected Waters Initiative Research Centre, UNSW Australia, Kensington, NSW 2052*
5 *Australia*

6 ²*Water Research Laboratory, School of Civil and Environmental Engineering, Manly Vale NSW 2093,*
7 *Australia*

8 ³*School of Geography, Earth and Environmental Sciences, University of Birmingham,*
9 *Edgbaston, Birmingham, B15 2TT, UK*

10 ⁴*School of Biology Earth and Environmental Sciences, UNSW Australia, Kensington, NSW*
11 *2052 Australia*

12

13 Corresponding author: Katie Coleborn

14 Email: k.coleborn@unsw.edu.au

15 Tel: +61434105636

16 **Abstract**

17 We present results of a detailed study of drip rate variations at 12 drip discharge sites in
18 Glory Hole Cave, New South Wales, Australia. Our novel time series analysis, using the
19 wavelet synchrosqueezed transform, reveals pronounced oscillations at daily and sub-daily
20 frequencies occurring in 8 out of the 12 monitored sites. These oscillations were not
21 spatially or temporally homogenous, with different drip sites exhibiting such behaviour at
22 different times of year in different parts of the cave. We test several hypotheses for the
23 cause of the oscillations including variations in pressure gradients between karst and cave
24 due to cave breathing effects or atmospheric and earth tides, variations in hydraulic
25 conductivity due to changes in viscosity of water with daily temperature oscillations, and
26 solar driven daily cycles of vegetative (phreatophytic) transpiration. We conclude that the
27 only hypothesis consistent with the data and hydrologic theory is that daily oscillations are
28 caused by solar driven pumping by phreatophytic trees which are abundant at the site. The
29 daily oscillations are not continuous and occur sporadically in short bursts (2-14 days)
30 throughout the year due to non-linear modification of the solar signal via complex karst
31 architecture. This is the first indirect observation leading to the hypothesis of tree water use
32 in cave drip water. It has important implications for karst hydrology in regards to developing
33 a new protocol to determine the relative importance of trends in drip rate, such as diurnal
34 oscillations, and how these trends change over timescales of weeks to years. This
35 information can also be used to infer karst architecture. This study demonstrates the
36 importance of vegetation on recharge dynamics, information that will inform both process-
37 based karst models and empirical estimation approaches. Our findings support a growing
38 body of research exploring the impact of trees on speleothem paleoclimate proxies.

39 **1. Introduction**

40 Karst architecture determines the flow and storage of water from the surface to the
41 underlying cave and is a major influence on drip discharge. Karst systems are characterised
42 by three principle flow types. Primary flow occurs where the water travels through the
43 primary porosity of the rock matrix, secondary flow pathways are characterised by water
44 transported along fractures in the bedrock and tertiary flow pathways consist of conduits
45 enlarged by dissolution. The dominance of a particular flow regime changes over time, for
46 example, older limestone tends to have higher secondary porosity (more fractures and
47 enlarged conduits) and a lower primary porosity due to compaction or cementation (Ford
48 and Williams, 1994). The relationship between karst architecture and delivery of water to
49 cave drip discharge sites has been studied to constrain uncertainty in paleoclimate studies
50 (Bradley et al., 2010; Markowska et al., 2015), identify suitable speleothems as climate
51 archives (McDonald and Drysdale, 2007) and in conjunction with drip water geochemistry to
52 determine water residence times in karst aquifers (Arbel et al., 2010; Fairchild et al., 2000;
53 Lange et al., 2010; Sheffer et al., 2011; Tooth and Fairchild, 2003; Treble et al., 2013b).
54 Recent research examining drip hydrology and fluctuations in drip rate have used

55 hydrological response to characterise flow paths. For example, Markowska et al., (2015)
56 used statistical analysis of drip hydrology data to identify storage flow, in both the epikarst
57 and overlying soil, to develop conceptual models of a karst system.

58 Over a timescale of months to years, fluctuations in drip discharge are typically driven by
59 seasonal variation in water availability (Hu et al., 2008; Sondag et al., 2003) and long-term
60 climate forcings such as the North Atlantic Oscillation or El Niño-Southern Oscillation
61 (McDonald, 2004; Proctor et al., 2000). On a daily to weekly timescale, drip rate responds to
62 individual rainfall events (Baldini et al., 2012) and barometric changes (Genty and Deflandre,
63 1998; Jex et al., 2012; Tremaine and Froelich, 2013). Tremaine and Froelich (2013) found
64 weekly and daily fluctuations at one drip site where an increase in barometric pressure
65 decreased volumetric drip rate. This was attributed to atmospheric tides, the heating and
66 cooling of the atmosphere, as the diurnal cycles occurred at two hours before the solar
67 noon (S1) and solar midnight (S2) each day. The cave was situated in poorly to moderately
68 indurated Oligocene limestone with a high likelihood of primary porosity (Scott, 2001). Jex
69 et al. (2012) observed a negative correlation between weekly barometric pressure changes
70 and drip rate at two out of forty drip sites monitored at the base of a paleokarst feature in
71 the marmorised and fractured Devonian limestone at Cathedral Cave, NSW. One drip
72 discharge site had a relatively strong anti-correlation ($R=-0.52$) after accounting for a 40 hr
73 time lag. This relationship was attributed to a two-phase flow, where pressure fluctuations
74 expanded and compressed air bubbles in the water held within the paleokarst in the
75 unsaturated zone.

76 Non-linear and chaotic behaviour of drip discharge has been observed over very short
77 (second to minutes) timescales. Chaotic drip regimes were first noted by Genty and
78 Deflandre (1998) in the Devonian limestone of southern Belgium (Genty and Deflandre,
79 1998). Chaotic and non-linear drip responses were also observed at an event-scale in the
80 fractured-rock limestone of Cathedral Cave, NSW (Mariethoz et al., 2012). These were
81 attributed to the filling and draining of subsurface karst stores within a recharge event, with
82 increasing homogenisation of flow with the filling of the stores. Baker and Brunston (2003)
83 observed non-linear responses to rainfall in multi-year drip time series from a fractured rock
84 (Carboniferous limestone) in Yorkshire, UK. With the exception of Tremaine and Froelich
85 (2013), daily fluctuations have not been observed in cave drip water hydrology.

86 In this paper we aim to increase our understanding of karst architecture by using a novel
87 approach, the wavelet synchrosqueezed transform, to analyse drip discharge time series
88 from 12 drip discharge sites in Glory Hole Cave, SE Australia. This analysis allows us to
89 characterise daily and sub-daily fluctuations in drip rate and identify the processes driving
90 these oscillations. This study has important implications for understanding karst
91 unsaturated flow processes and karstic groundwater recharge. Currently, most karst models
92 use very simplistic representations of unsaturated flow, if it is considered at all (Hartmann et
93 al., 2014a). This study highlights the importance of vegetation dynamics on vadose flow and

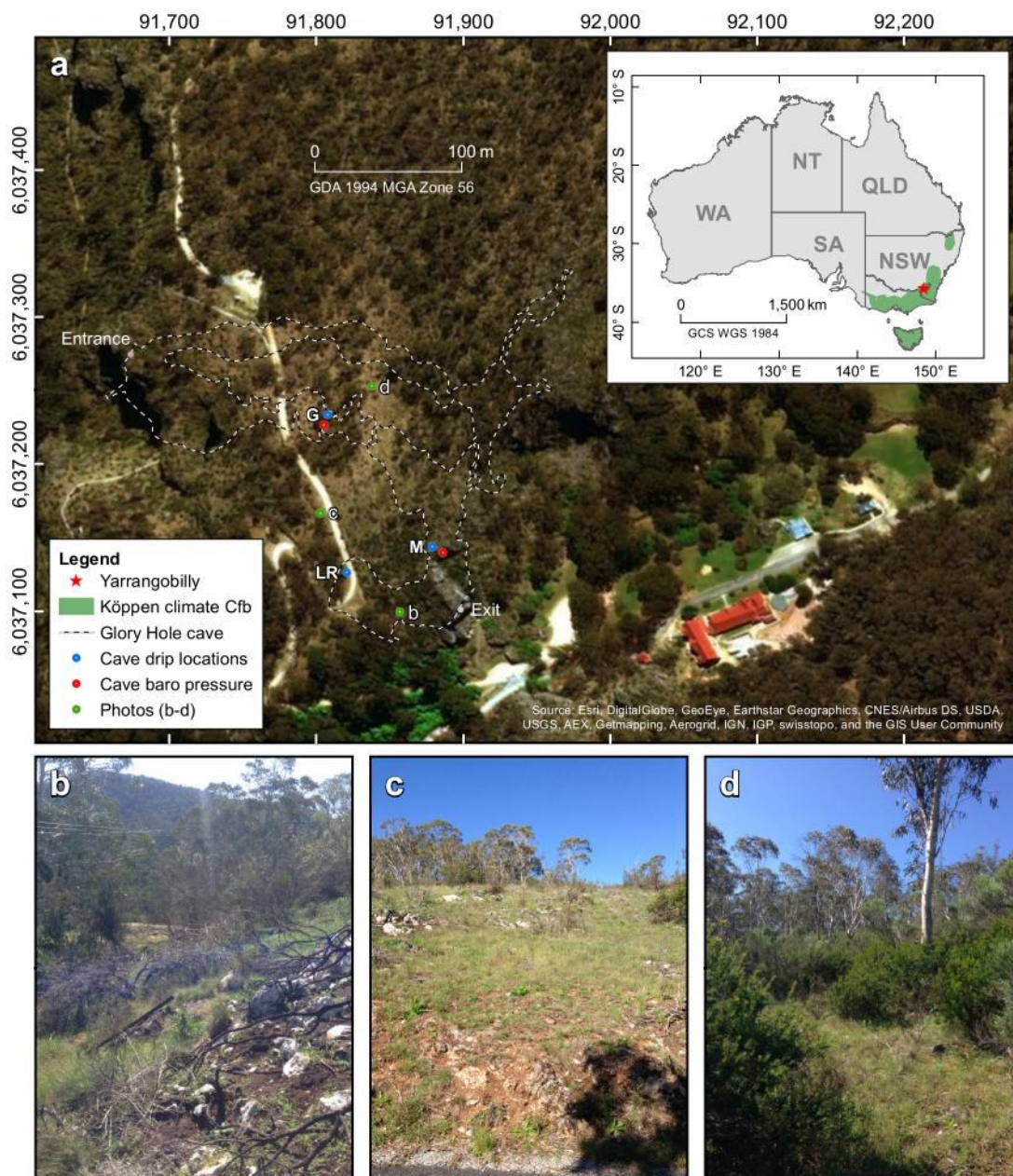
94 recharge making it significant to karst modelling research and speleothem-based
95 paleoclimate studies which focus on the impact of vegetation dynamics on proxy records
96 (Treble et al., 2015, 2016)

97

98 **2. Field site and methods**

99 **2.1 Glory Hole Cave at Yarrangobilly Caves National Park**

100 Glory Hole Cave is part of the Yarrangobilly Caves National Park located in the Snowy
101 Mountains, New South Wales, Australia (35°43'29.3"S 148°29'14.9"E) at an elevation of 980
102 m (Australian Height Datum). The Snowy Mountains forms part of the Great Dividing Range,
103 a mountainous region stretching along the eastern seaboard from Queensland to Victoria.
104 The region is sub-alpine and the climate is classified as temperate montane with mild
105 summers and no dry season (Köppen climate classification Cfb) (Peel et al., 2007; Stern et
106 al., 2012).



107

108 Figure 1: Location of Yarrangobilly Caves in New South Wales, Australia with photos of
109 surface vegetation b-d. Extent of Köppen climate zone is from Peel et al. (2007).

110 Glory Hole Cave is formed of two main sections connected by a narrow constriction ~2 m x 6
111 m. It is ~243 m in length and is ~100 m at its widest point. The cave extends more than 40 m
112 below the surface in an unsaturated zone of westward sloping limestone bedrock with a
113 contributing catchment area of ~1 km². The cave is situated within a formation of massive
114 limestone approximately 12 km long and on average 1 km wide (Worboys, 1982). The
115 limestone is typical of south-eastern Australian limestone; it is Silurian, highly fractured and
116 marblised with little primary porosity. The bedding planes of the limestone are generally
117 obvious with a westward dip (Adamson and Loudon, 1966). It is likely that Glory Hole Cave
118 was formed by water running off less permeable rocks to the east of the limestone, sinking
119 to the water table and rising through large springs close to the Yarrangobilly River (Spate,
120 2002) which is situated in a gorge in <100 m west of the cave entrance. Glory Hole Cave is
121 likely to be relevant for paleoclimate proxies as there is an abundance of speleothems and
122 in close proximity (<100 m) to caves that have been used in multi-proxy speleothem based
123 paleoclimate studies (Markowska et al., 2015; Webb et al., 2014).

124 The vegetation is classified as sub-alpine open snowgum (*Eucalyptus pauciflora subsp.*
125 *pauciflora*) and black sallee (*E. stelullata*) woodland.

126

127 **2.2 Cave and surface monitoring**

128 Drip discharge rate was recorded at 12 drip sites in three locations (Fig. 1 and Table 1)
129 within Glory Hole Cave using Stalagmate[®] drip loggers between December 2012 and
130 September 2015, and monitoring is ongoing. The drip sites were chosen using a stratified
131 sampling method. A transect of the cave was used to select three locations (G, M and LR)
132 that satisfied the following criteria 1) there were actively dripping speleothems, 2) spatially
133 distant from the other locations and 3) different depths within the cave. Individual drips
134 were sampled randomly at each location, with selection guided by practical constraints such
135 as stalagmite surface being suitable for placement of logger and the drip falling from high
136 enough to activate pressure sensor on the logger. Drip loggers recorded the frequency of
137 drips falling onto the surface of the sealed box containing an acoustic sensor in 15 min
138 intervals. The number of drips were converted to ml min⁻¹, assuming that 1 drip equals 0.19
139 ml (Collister and Matthey, 2008; Markowska et al., 2015). Recently, automated drip loggers
140 have been widely used in cave hydrology research (Cuthbert et al., 2014b; Hu et al., 2008;
141 Mahmud et al., 2015; Rutledge et al., 2014; Treble et al., 2013a) as they provide a more
142 convenient and efficient way of recording higher temporal resolution data than traditional
143 drip counting methods.

144

145 Table 1: Summary of drip sites and location within cave as indicated in Fig. 1, the monthly
 146 mean and standard deviation (std) of total flow volume and maximum and minimum drip
 147 rate in summer (December- February) and winter (June- August).

Site	Location	Total flow volume (L)				Drip rate (ml min ⁻¹)			
		Summer		Winter		Summer		Winter	
		mean	std	mean	std	Maximum	Minimum	Maximum	Minimum
G1	G	72.67	9.21	209.58	107.78	19.51	1.84	56.75	0.00
G3		23.76	10.13	115.44	8.37	7.00	0.00	34.43	0.00
G6		3.73	1.90	16.45	0.10	1.43	0.10	4.10	0.65
G8		6.36	0.49	5.81	0.16	1.11	0.00	0.96	0.34
G10		32.47	23.08	104.54	73.58	9.97	0.04	27.27	0.00
G12		6.57	5.71	9.74	4.39	1.68	0.00	2.04	0.43
LR1	LR	32.31	23.93	98.62	7.39	58.30	0.00	57.77	0.00
M1	M	0.29	0.18	0.47	0.00	0.13	0.00	0.11	0.00
M2		7.67	12.85	120.09	21.21	42.53	0.00	74.30	0.00
M4		0.88	1.47	33.95	5.17	4.02	0.00	28.45	0.00
M10		24.53	34.68	127.79	51.36	13.95	0.00	27.56	0.00
M13		7.33	5.05	67.03	6.60	12.40	0.09	41.80	0.92

148

149 Barometric pressure and air temperature were recorded at two locations within the cave
 150 (Fig. 1) using Solinst level loggers at 15 min intervals from January-September 2015.
 151 Precipitation (accuracy $\pm 4\%$ of total mm), wind speed (accuracy ± 0.1 kph), relative
 152 humidity (accuracy $\pm 2\%$), air temperature (accuracy ± 0.5 °C) and barometric pressure
 153 (accuracy: ± 1.0 kPa) were measured with a Davis Vantage Pro 2 weather station <1 km from
 154 Glory Hole Cave at 15 min intervals and data stored using a Datalogger DT80 data logger.
 155 Solar radiation ($W m^{-2}$) was derived from satellite imagery processed by the Bureau of
 156 Meteorology from the Geostationary Meteorological Satellite and MTSAT series.

157 Daily potential evapotranspiration was estimated using “ETo Calculator” software
 158 developed by the Land and Water Division of the Food and Agriculture Organisation of the
 159 United Nations <http://www.fao.org/nr/water/eto.html>. The software is based on the
 160 Penman-Monteith equation and is a physically-based method with physiological and
 161 aerodynamic parameters. The climate parameters used were air temperature (mean,
 162 maximum and minimum), relative humidity (mean, maximum and minimum), wind speed
 163 and solar radiation.

164

165 2.3 Spectral analysis of cave drip discharge rates

166 A new advance in signal processing was used to analyse the time-frequency content of
 167 measured cave drip discharge rate, temperature and barometric pressure. Here, the
 168 frequencies of interest are 1 cycle per day (cpd) and faster, i.e. diurnal to sub-diurnal.

169 Daubechies et al (2011) first presented the wavelet synchrosqueezed transform (WSST) as
 170 an empirical mode decomposition like tool for disentangling an amplitude and phase
 171 modulated signal into approximately harmonic components. Thakur et al (2013) adapted
 172 the WSST to discretised data (rather than continuous functions) and developed a MATLAB®
 173 Synchrosqueezing Toolbox (available for download:
 174 <https://web.math.princeton.edu/~ebrevdo/synsq/>) which efficiently implements the WSST
 175 algorithm and offers a log2 frequency resolution (WSST was officially implemented in
 176 MATLAB® as of release R2016a). They further tested the robustness properties of WSST and
 177 found that it precisely estimated key signal components, and that it was stable against
 178 errors and noise (Thakur et al., 2013). The WSST combines advantages of the wavelet
 179 transform in regards to frequency resolution with the frequency reallocation method (Auger
 180 and Flandrin, 1995) in order to reduce spectral smearing when mapping out the time-
 181 frequency content of a complicated signal.

182 The drip discharge rate time series, barometric pressure and air temperature (potential
 183 weather related drivers of drip discharge oscillations) were analysed for time-frequency
 184 content in the following way:

- 185 • Application of the WSST functions in MATLAB® (version R2016a or later) or the
 186 Synchrosqueezing Toolbox (Thakur et al, 2013) to compute the signal's frequency
 187 content over time. The output is a 2D matrix containing the complex frequency domain
 188 response $\mathcal{F}_{f,t}$ with elements corresponding to discrete frequency and time values (e.g.,
 189 as rows and columns). Here, f is frequency (in \log_2 resolution) $[1/T]$ and t is discrete
 190 time (sampling resolution) $[T]$.

- 191 • Calculation of the component amplitudes according to the standard signal processing
 192 procedure using

$$193 \quad A_{f,t} = |\mathcal{F}_{f,t}| = \sqrt{\Im(\mathcal{F}_{f,t})^2 + \Re(\mathcal{F}_{f,t})^2} \quad (1)$$

- 194 • Normalisation of the component amplitudes using

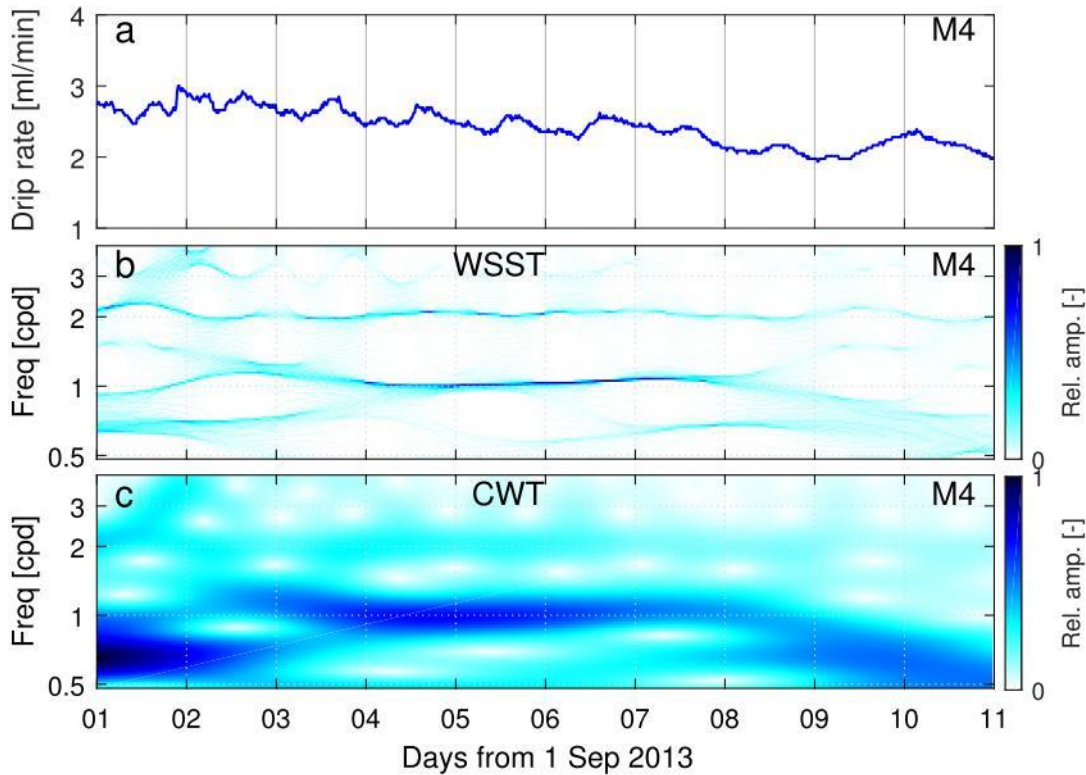
$$195 \quad a_{f,t} = \frac{A_{f_{min}<f<f_{max},t}}{\max(A_{f_{min}<f<f_{max},t})} \quad (2)$$

196 In order to highlight the main frequency components of interest (1 and 2 cpd) we chose
 197 $f_{min} = 0.5$ and $f_{max} = 4$ for the normalisation. However, for other applications
 198 different frequency limits could be useful to identify continuous periods of weaker
 199 frequency components in the presence of other, stronger components as well as chaos.

- 200 • Visualisation of the normalised amplitude matrices in pseudo-colour plots. Distinct
 201 frequency components (signals with contrasting amplitudes whose frequency does not
 202 significantly change over time) can easily be distinguished from chaos (i.e., lack of
 203 regular oscillations identified as signals with varying amplitude and frequency over
 204 time). Stronger periodic components would yield larger amplitudes and therefore also a
 205 value that is closer to 1 in the respective WSST plots. While this analysis is conducted

206 manually, it could be automated using criteria for the strength, continuity and stability
207 of any frequency component of interest.

208



209

210 Figure 2: Comparing the time-frequency content of the drip discharge rate (a) for drip site
211 M4 (refer to Figure 3): Relative component amplitudes calculated from (b) the wavelet
212 synchrosqueezed transform (WSST), and (c) the continuous wavelet transform (CWT) using a
213 Morlet mother wavelet.

214 An example of the time-frequency mapping conducted according to the above described
215 method is illustrated in Figure 2. The results obtained by applying the WSST (Figure 2b) can
216 be compared to the results from a continuous wavelet transform (CWT) with a Morlet
217 mother wavelet (Figure 2c) (Torrence and Compo, 1998). From this example it is clear that
218 WSST features significantly less time-frequency smearing and therefore allows improved
219 identification and delineation of close-by frequency components such as those at 1 or 2 cpd
220 (compare Figures 2b and 2c). Therefore, WSST presents a significant advantage over
221 traditional signal processing methods such as the continuous wavelet transform when
222 identifying the timing and duration of multiple frequency components embedded in
223 measurements.

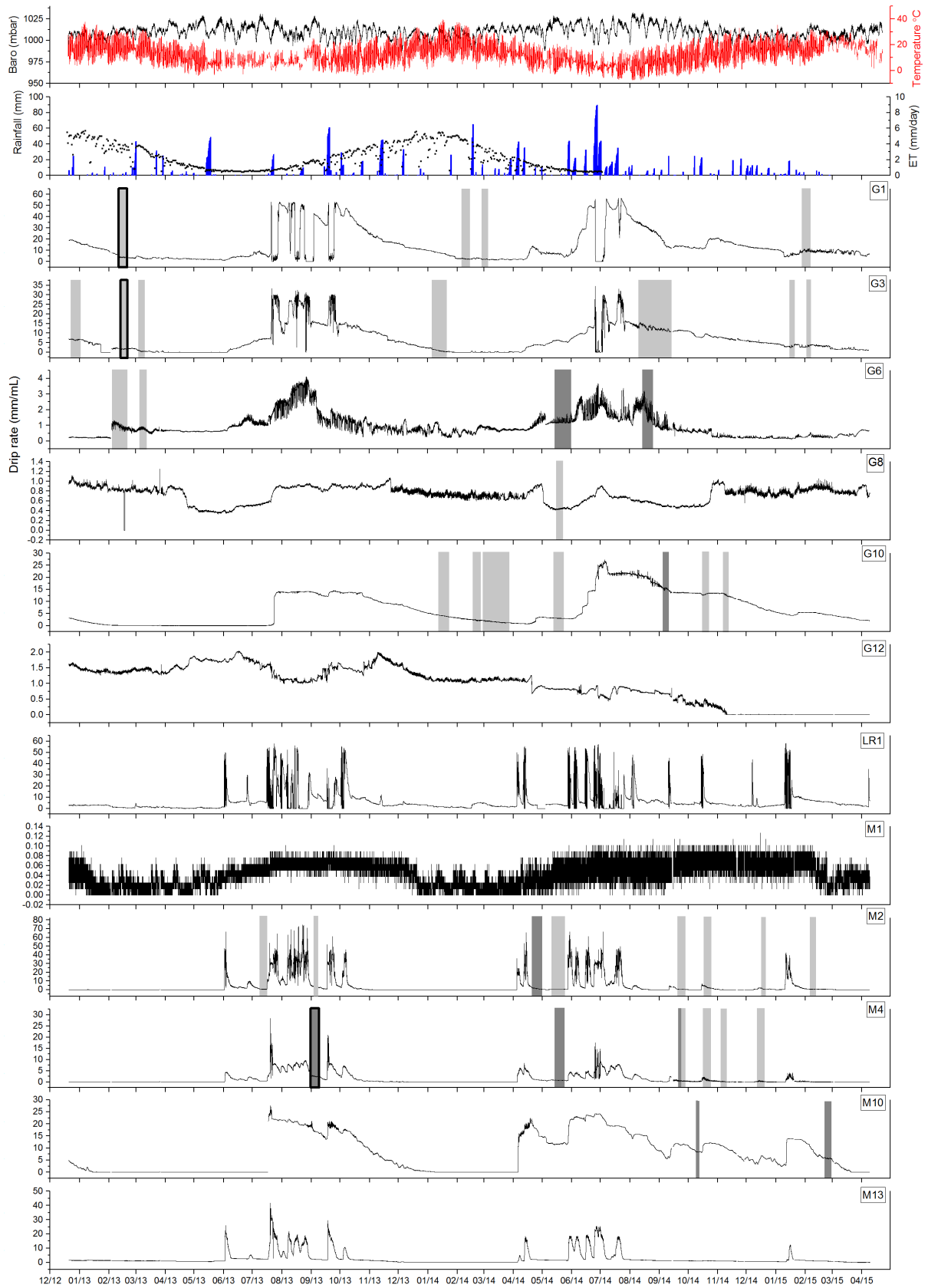
224 Using this methodology, a periodic drip discharge rate could be defined as consisting of
225 continuous periods of a) stable 1 cpd frequency, b) stable 1 cpd and 2 cpd frequency, c)
226 chaos (components with randomly varying frequency and amplitude). We used a) and b) as

227 spectral “fingerprints” to identify and mark periods of continuous occurrence of daily and
228 sub-daily oscillations in the drip discharge rate dataset.

229 **3. Results**

230 **3.1 Drip discharge rate time series**

231 The drip discharge time series are presented in Fig. 3. The drip discharge sites are spatially
232 clustered in three groups within the cave (Fig. 1 and Table 1). Sites with the G prefix are
233 located near the main entrance of the cave on the western side. The location is highly
234 decorated with speleothems. M sites are located in the middle section of the cave in a large
235 chamber with a high ceiling populated by soda straw formations. Location LR1 is situated
236 near the cave exit at the top of a flow stone.



237

238

239 Figure 3: Drip discharge rate time series for all drip sites in Glory Hole Cave with periods
240 where daily fluctuations occur highlighted in light grey (1 cpd) and dark grey (1 cpd and 2
241 cpd). The time periods examined in more detail in Fig. 4, 5 and 6 are indicated by bolder
242 outline. Daily evapotranspiration (19/12/2012- 03/07/2014), rainfall, barometric, air
243 temperature and are also shown.

244 The drip discharge rate at G1 and G3 varies seasonally, with higher drip rates in winter, total
245 flow volume of 133.37 L and 109.52 L, respectively, than summer (64.56 L and 14.1 L,
246 respectively). Drip rate increases in response to rainfall events during the wet season and
247 gradually decreases through the drier part of the year. Drip rate is lowest during April and
248 May and highest during June and July. Similarly, G6 exhibits seasonal variation with a higher
249 volume of discharge during the winter than summer. The drip rate at G10 increases sharply
250 from 0.14 ml min⁻¹ on 21/07/2013 to 13.75 ml min⁻¹ on 29/07/2013, this drip rate is
251 consistently sustained for 3 months indicated by the flat topped hydrograph (Fig. 3). From
252 July 2013 onwards, the drip rate gradually decreases until June 2014 where it increases
253 sharply again by an order of magnitude from 2.03 ml min⁻¹ on 3/06/2014 to 24.96 ml min⁻¹
254 on 4/07/2014. In May 2014, the drip rate again rapidly increases at G10 from 0.142 ml min⁻¹
255 to 21.59 ml min⁻¹ on 18/04/2014 and then proceeds to gradually decline until April 2015
256 where it reaches baseline conditions. M10 exhibits similar behaviour with a low baseline
257 drip rate which increases sharply during July 2013 and is sustained for ~3 months, however,
258 the elevated drip rate decreases more rapidly than G10, returning to baseline conditions in
259 January 2014. M1 has a very low drip rate ranging from 0- 0.13 ml min⁻¹ and is seasonally
260 variable with higher drip rates during the winter. LR1, M2, M4 and M13 are very responsive
261 to infiltration events and are characterised by a 'flashy' flow type, evidenced by the
262 frequent spikes in drip rate. G12 has a low discharge rate which gradually decreases over
263 the monitoring period until the site dries up completely in November 2014. There are small
264 variations in drip rate that are not associated with rainfall events or seasonal drying. G8 is
265 the only site which has a lower total flow volume during the winter (2013= 5.92 L; 2014= 5.7
266 L) than summer (2014= 6.39 L; 2015= 6.84 L).

267

268 **3.2 Characterisation of oscillations in the drip discharge rate**

269 Daily fluctuations in drip discharge rate were identified in eight out of twelve sites using
270 WSST. There was no connection between the sites that did not exhibit the fluctuations with
271 respect to spatial location, flow volume or flow regime type. The temporal and spatial
272 pattern of daily oscillations are shown by the grey shaded areas in Fig. 3. The length of time
273 the signal is present varied temporally for each drip site. For example, there was a strong 1
274 cpd signal in the drip water at G1 for 10 days in February 2013 whereas in January 2014 1
275 cpd fluctuations only lasted 5 days (Fig. 4). The timing of when the signal occurs on an
276 annual scale varied within and between drip sites. For example, a 1 cpd signal only occurred
277 during the first 3 months of the year for G1, whereas a 1 cpd signal occurred sporadically at

278 G3 throughout the calendar year (December 2012, February and March 2013, January 2014,
 279 September 2014, January 2015).

280 The daily timing of minimum and maximum drip rate varied within and between individual
 281 drip sites. At G1 the 1 cpd maximum and minimum drip rate generally around 6am-12pm
 282 and 12-9pm, respectively. Daily oscillations were only observed once at G8 between 14-
 283 21/05/2014 with minimum drip rate at 3-9 am and maximum drip rate around 12-9pm. Both
 284 1 cpd and 2 cpd signals were observed at M10 for all the periods of drip rate oscillation with
 285 the larger peak occurring in the afternoon around 3-6 pm , minimum drip rate appeared
 286 consistently between 6-9 am. Time lag between air temperature and drip rate was
 287 quantified by performing a cross correlation analysis with a shift interval of 15 mins up to
 288 ± 24 hours (Table 2). The lag time was identified as the point of maximum negative
 289 correlation between the two variables with the exclusion of sites with missing data. At most
 290 sites the lag time between maximum air temperature and minimum drip rate varied greatly
 291 over the monitoring period. For example, at M4 initially the lag time was 24 hours in
 292 September 2013, decreasing to 9 hours in May 2014 and eventually levelling off at around
 293 16 hours from September to December 2014. In contrast, G1 had a similar lag time over all 4
 294 periods of drip rate fluctuation ranging from 11.25- 12.75 hours. G6 was unique in that the
 295 minimum drip rate occurred before the maximum air temperature in February and March
 296 2013, January 2014 and 2015. Analysis of variance indicated that drip site and season did
 297 not explain a significant amount of variance in lag time.

298

299 Table 2: The time lag calculated using cross correlation analysis between air temperature
 300 and daily drip rate for each period of drip rate oscillation, the timing of when minimum and
 301 maximum drip rate occurred within the time periods * denote periods where a 2cpd signal
 302 occurs. A negative time lag means the minimum drip rate lags behind the peak temperature
 303 whereas a positive lag means the minimum drip rate precedes the maximum temperature.

Site	Drip rate oscillation period		Time lag (hours)	R ² (p-value<0.05)	Max drip rate	Min drip rate
	Start	End			from-to	from-to
G1	11/02/2013	21/02/2013	-11.5	-0.82	09:00-12:00	18:00-21:00
	4/02/2014	14/02/2014	-12.75	-0.55	09:00-12:00	18:00-21:00
	27/02/2014	10/03/2014	-11.25	-0.37	09:00-12:00	12:00-21:00
	27/01/2015	5/02/2015	-11.5	-0.69	06:00-12:00	12:00-21:00
G3	23/12/2012	2/01/2013	-23.25	-0.46	12:00-00:00	00:00-09:00
	12/02/2013	20/02/2013	2	-0.56	15:00-00:00	06:00-15:00
	4/03/2013	10/03/2013	1	-0.44	15:00-00:00	03:00-09:00
	6/01/2014	20/01/2014	7	-0.62	00:00-09:00	12:00-18:00
	20/09/2014	29/09/2014	-4	-0.38	09:00-18:00	03:00-06:00
	16/01/2015	20/01/2015	0.25	-0.59	18:00-21:00	03:00-09:00
	3/02/2015	6/02/2015	1	-0.74	15:00-21:00	06:00-09:00

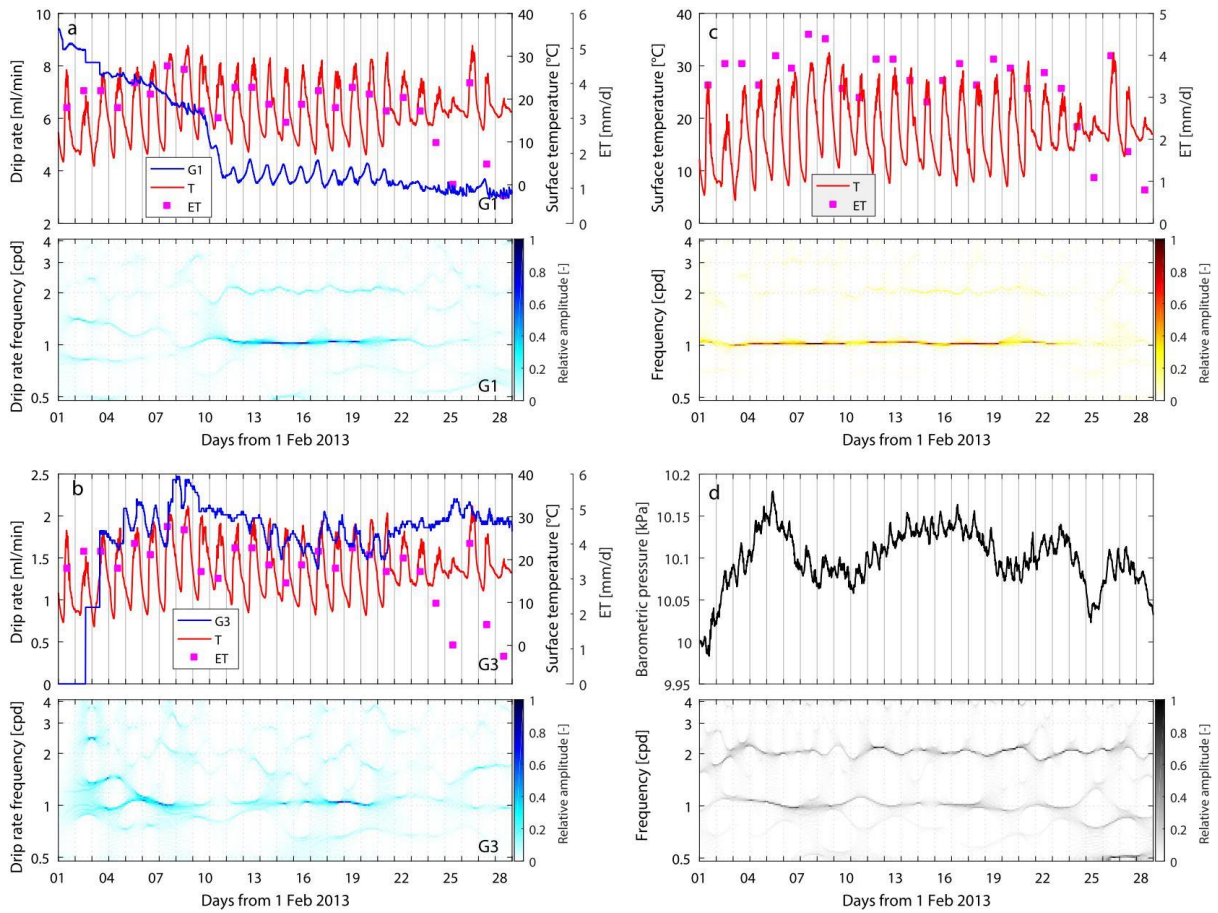
G6	3/02/2013	19/02/2013	-4	-0.19	18:00-00:00	03:00-06:00
	5/03/2013	12/03/2013	-3.25	-0.51	15:00-21:00	03:00-09:00
	13/05/2014	29/05/2014*	-21	-0.5	15:00-18:00	03:00-06:00
	14/08/2014	24/08/2014*	-7	-0.5	15:00-18:00	21:00-00:00
G8	14/05/2014	21/05/2014	-9.5	-0.55	12:00-21:00	03:00-09:00
G10	5/10/2013	16/10/2013*	-24	-0.4	15:00-18:00	03:00-06:00
	5/01/2014	22/01/2014	-0.5	-0.32	15:00-21:00	03:00-06:00
	18/02/2014	24/02/2014	-3	-0.46	15:00-21:00	21:00-00:00
	4/03/2014	23/03/2014	-2.75	-0.47	15:00-18:00	03:00-09:00
	13/05/2014	23/05/2014	-15	-0.37	15:00-00:00	00:00-06:00
	16/10/2014	22/10/2014*	-23	-0.49	15:00-21:00	06:00-09:00
	8/11/2014	12/11/2014	-1.5	-0.59	18:00-21:00	06:00-09:00
	5/02/2015	25/02/2015	-0.25	-0.33	15:00-21:00	06:00-09:00
M2	3/09/2013	7/09/2013	-15.25	-0.76	15:00-18:00	06:00-09:00
	20/04/2014	28/04/2014*	-1	-0.4	00:00-03:00	06:00-09:00
	13/05/2014	21/05/2014	-17.75	-0.6	15:00-18:00	06:00-09:00
	20/09/2014	28/09/2014	-23.75	-0.4	15:00-18:00	06:00-09:00
	18/10/2014	25/10/2014	-2	-0.31	15:00-18:00	06:00-09:00
	5/02/2015	10/02/2015	-20.75	-0.51	00:00-03:00	12:00-15:00
M4	2/09/2013	8/09/2013*	-24	-0.46	12:00-18:00	06:00-09:00
	14/05/2014	23/05/2014*	-9	-0.38	15:00-18:00	06:00-09:00
	16/10/2014	24/10/2014	-16.25	-0.65	00:00-12:00	12:00-21:00
	4/11/2014	13/11/2014	-16.5	-0.62	21:00-03:00	12:00-21:00
	12/12/2014	22/12/2014	-16.5	-0.32	00:00-09:00	18:00-21:00
M10	23/12/2012	26/12/2012*	-24	-0.32	15:00-18:00	09:00-12:00
	9/10/2014	12/10/2014	-4.75	-0.46	15:00-18:00	09:00-12:00

304

305

306 1 cpd and 2 cpd signals can occur concurrently, for example, at M4 between 1-9/9/2013
307 (Fig. 5). This trend, where the 2 cpd is weaker than the 1 cpd is consistent across all sites
308 where the two signals coincide. The 2 cpd signal can be visually determined in the raw drip
309 rate data by a second smaller peak). Examples of characteristic WSST plots alongside the
310 corresponding raw drip rate and surface temperature data will be discussed in greater detail
311 below. All WSST analyses have been plotted in the SI.

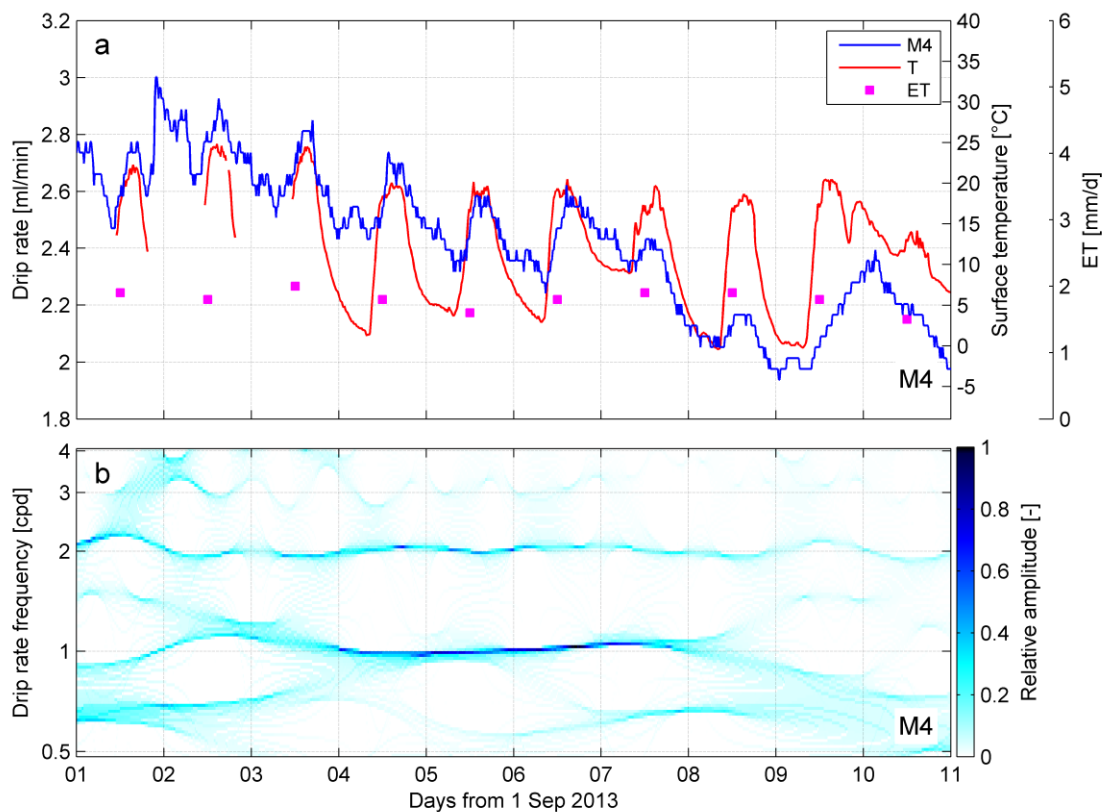
312



313

314 Figure 4: The raw drip rate, evapotranspiration and surface temperature data with the
 315 corresponding drip rate WSST plot for time periods where a 1 cpd signal is present for sites
 316 a) G1 and b) G3 c) surface air temperature (T) and potential evapotranspiration (ET) and d)
 317 barometric pressure for period February 2013.

318



320

321 Figure 5: The raw drip discharge data, evapotranspiration, surface temperature and wavelet
 322 synchrosqueezed transform (WSST) plot of the drip discharge for site M4 from 1-
 323 11/09/2013.

324 WSST identified a 1 cpd oscillation in drip rate between 08/02/2013 and 21/02/2013 at G1
 325 and G3 (Fig. 4a, b). At G1 (Fig. 4a), the signal was initially chaotic, but from 08/02/13-
 326 21/02/13 the drip rate oscillates sharply at 1 cpd. The maximum drip rate ranging from 4.03-
 327 3.75 ml min⁻¹ occurred between 9:18 and 10:27 and the minimum drip rate ranging from
 328 3.34 -3.75 ml min⁻¹ occurred between 18:39 and 21:27. The signal was chaotic from
 329 21/02/2013.

330 The drip rate at G3 (Fig. 4b) oscillated at 1cpd for 8 days from 12/02/13-20/02/13. In
 331 contrast to G1, the maximum drip rate appeared in the evening and the minimum drip rate
 332 occurred in the morning. The maximum drip rate ranging from 1.63 -2.01 ml min⁻¹ occurred
 333 between 20:21 and 00:40 and the minimum drip rate ranging from 0.36-0.48 ml min⁻¹
 334 occurred between 9:03 and 11:36 with the exception of 15/02/13 and 18/02/13 where it
 335 appeared at 14:06 and 12:57, respectively. Similar to G1, the 1 cpd trend descended into
 336 chaos from 20/02/13 onwards. The maximum drip rate occurs between 14:23 and 22:45 and
 337 ranged from 0.53 to 1.14 ml min⁻¹. The minimum drip rate occurred between 01:18 and
 338 11:32 and ranged from 0.228 to 0.95 ml min⁻¹.

340 From 01-27/02/13, daily barometric pressure peaked between 8:30-9:00 with a magnitude
341 of 0.1-0.5 kPa with a smaller second peak between 20:00-22:00 with a magnitude of 0.1-0.3
342 kPa (Fig. 4c). There were larger changes in air pressure on a mesoscale with peaks in air
343 pressure on 16/02/13, 22/02/13, 26/02/13 and minimum air pressure on 19/02/13,
344 24/02/13 and 28/02/13. The air pressure changes in these cycles were as much as 1.5-2 kPa.
345 The drip rate at G1 and G3 did not appear to be affected by the daily or weekly changes in
346 air pressure. For example, when air pressure decreased dramatically on 27/02/13 (Fig. 4c)
347 there was no substantial change in drip rate at either G1 or G3.

348 Insolation drives daily cycles in surface air temperature with maximum temperatures
349 recorded between 11:30-16:00 and minimum temperatures recorded between 4:00-8:00
350 (Fig. 4d). The difference in daily minimum and maximum air temperature varied greatly. For
351 example, between 12- 20/02/2013 the difference was 17.05-22.2 °C whereas between 21-
352 27/02/2013, the temperature difference was as little as 4.5 °C. Evapotranspiration ranged
353 from 0.8- 4.5 mm/day and was relatively high from 1-23/02/2013 with a slight downward
354 trend which then decreased sharply on 23/02/2013 and 24/02/2013 to 2.3 mm/day and 1.1
355 mm/day, respectively.

356 **4. Discussion**

357 **4.1 Cave drip rate and karst architecture**

358 The complexity of the Glory Hole Cave karst system is evident in the variety of drip regimes.
359 For example, the drip rate at G1, G6 and G3 is seasonally driven with high discharge rates
360 during the wettest period of the year. In contrast, drip discharge at G10 and M10 is likely
361 driven by a storage component which discharges via a less permeable pathway which limits
362 the store at a particular level during wet periods. The drip site is fed via the main water
363 store rather than the overflow pathway itself (Baker et al., 2012; Bradley et al., 2010). Sites
364 LR1, M4, M13 and M2 behave similarly in that they are all very responsive to rainfall events
365 and have low base flows during periods of low rainfall. The response to rainfall events occur
366 within 24 hours across these sites. Calculated flow volumes indicate the storage capacity of
367 the stores feeding the discharge sites. For example, there was an infiltration event on
368 01/06/2013 which caused a dramatic increase in drip rate for sites LR1, M2, M4 and M13.
369 The flow volumes for each site from the start of the event to the point where the discharge
370 returns to a constant rate are as follows LR1 (1.60 L), M4 (2.99 L), M13 (8.09 L) and M2
371 (11.30 L). The length of the recession limb, calculated from the peak of the hydrograph until
372 the drip rate returns to base rate, is indicative of the speed at which the store drains. For
373 example, the decay in drip rate is 12 days for site M2 compared to 4 days for M13. The time
374 it takes for the store to drain is not dependent on flow volume, as M13 has a flow volume of
375 more than 5 times that of site LR1 but they both have drainage periods of 5 days. The
376 discrepancy in drainage time could indicate variation in flow pathway length between sites.
377 G8 is the only site with a relatively lower total flow volume during winter than summer. M1
378 has a low drip rate that shows a small seasonal fluctuation but does not visibly respond to
379 individual events. This site is likely being fed by a store that is large enough to assimilate
380 short term inputs from the surface without impacting drip rate. This type of store has been
381 described as a karst hydrological model component in a number of studies (Arbel et al.,
382 2010; Hartmann et al., 2014b; Markowska et al., 2015).

383

384 **4.2 Daily oscillations in drip rate**

385 Constant frequency oscillations in drip discharge (1 cpd and 2 cpd) occur sporadically
386 throughout the monitoring period December 2012- April 2015 at 8 out of 12 monitored drip
387 sites. This phenomenon could be explained by a number of daily drivers including variations
388 in pressure gradients between karst and cave due to cave ventilation effects, atmospheric
389 and earth tides, or variations in hydraulic conductivity (due to changes in viscosity of water
390 with daily temperature oscillations), and solar driven daily cycles of vegetative
391 (phreatophytic) transpiration. These drivers are now considered in turn.

392

393 **4.2.1. Cave ventilation effects**

394 Surface air pressure and cave air pressure were significantly correlated ($\tau= 0.82$ significant at
395 95%, $n=8939$) for the monitoring period 19/01/2015-08/09/2015. This indicates that cave air
396 exchange (“breathing” or ventilation) is very efficient and consequently that variations in air
397 pressure between the cave and surface can be ruled out as driving the fluctuations in drip
398 rate.

399

400 **4.2.2. Barometric loading**

401 Atmospheric tides are caused by changes in air pressure due to the heating and cooling of
402 air masses during the day and night. Correlations between atmospheric tides and drip rates
403 can occur since increases (decreases) in atmospheric pressure at the ground surface are
404 partitioned into stress increase (decrease) in the soil/rock mass and pore pressure increase
405 (decrease) within the formation (Acworth et al., 2015). Drip rates could be affected if this
406 changes the pressure gradient between the groundwater in karst stores and the cave
407 (Tremaine and Froelich, 2013). Such a pressure imbalance is dependent on the
408 hydromechanical properties and karst architecture as well as the degree of pneumatic
409 connection between both the surface and the water table, and the surface and the cave at
410 the location of the drip. Maximum and minimum atmospheric pressure occur at the same
411 time each day (Fig. 4d).

412 Atmospheric tides were eliminated as a process to explain the daily oscillation phenomenon
413 for several reasons. Firstly, there was no relationship between drip discharge rate and the
414 longer term barometric changes caused by synoptic weather patterns (Fig. 4). The
415 mesoscale fluctuations in pressure caused by synoptic weather patterns are an order of
416 magnitude higher than those caused by daily atmospheric tides. Since the drip rate did not
417 respond to pressure changes of this size, they will not respond significantly to changes of a
418 smaller magnitude at a higher frequency because higher frequency signals will be more
419 highly damped and lagged. Secondly, the timing of the daily maximum and minimum drip
420 rates in Glory Hole Cave varied within each drip site over time. For example, the peak
421 discharge time for site G6 varied between 13:24 and 19:48 for the period 11/08/2013-
422 25/08/2015. This finding contrasts with previous studies where drip rate is negatively
423 correlated with barometric pressure and responds to daily pressure changes linearly
424 (Tremaine and Froelich, 2013). However, this could indicate that the daily drip water
425 variations in Glory Hole Cave are being driven by a non-linear process and this is discussed
426 further below. Thirdly, the karst architecture of Glory Hole Cave is well-developed, has little
427 to no primary porosity and is unconfined. Hence, it is unlikely to exhibit barometric
428 responses such as seen in confined systems (Merritt, 2004), whereby pore pressure changes
429 due to barometric loading are substantially lower than the change of cave air pressure.

430

431 **4.2.3. Earth tides**

432 Earth tides are solid deformations of the Earth's surface caused by the gravitational pull of
433 the moon and sun (Merritt, 2004). It has been previously shown that earth tides can cause
434 regular oscillations in groundwater level if the aquifer is sufficiently confined (Acworth et al.,
435 2015). However, at Glory Hole Cave this process can be ruled out due to the unconfined
436 conditions, the fact that the compressibility of limestone is smaller than that of water, and
437 because fluctuations in pressure caused by earth tides are so small.

438

439 **4.2.4. Temperature driven viscosity influences on hydraulic conductivity**

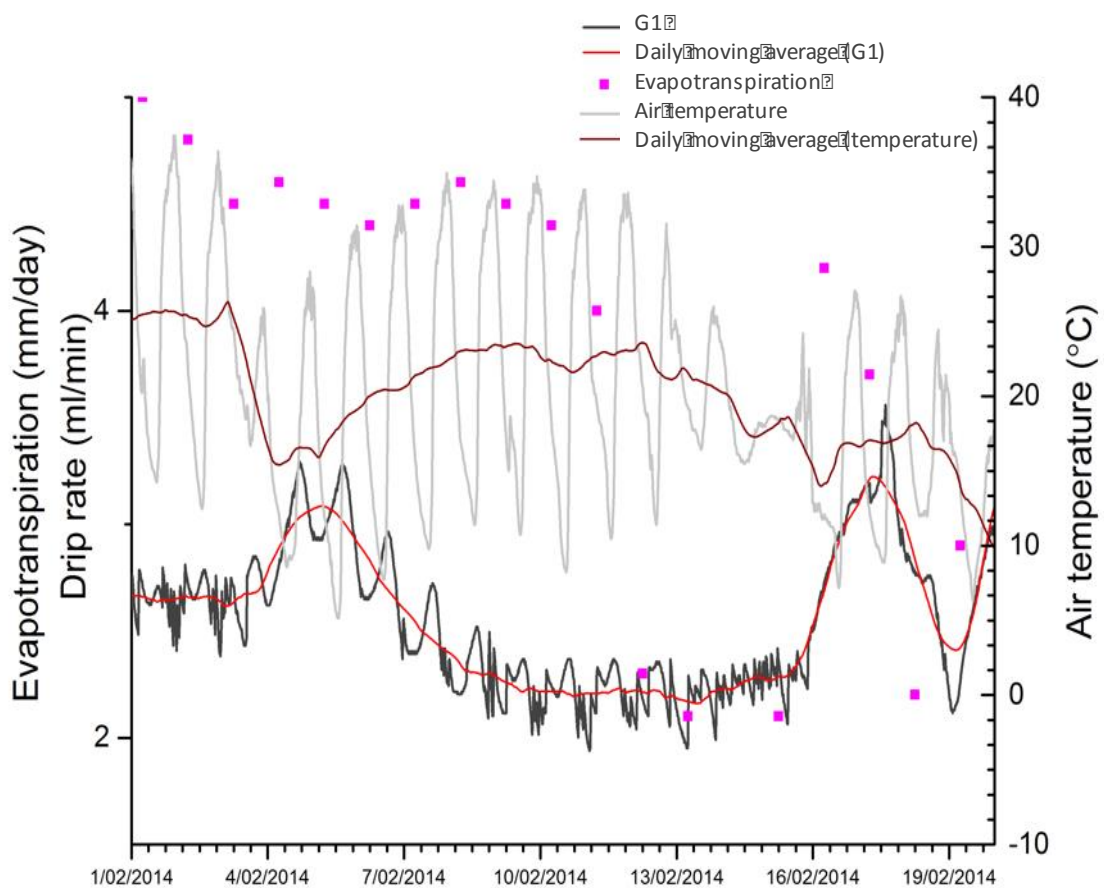
440 The study site has large surface temperature variations, particularly in summer where day
441 time and night time temperatures can vary up to 31.1 °C. Consequently, the dynamic
442 viscosity of water could range from 0.8- 1.79 x 10⁻³ Pa s (based on a temperature range from
443 30-0 °C, respectively). However, the conductive propagation in diel temperature variations
444 are expected to be highly attenuated with depth (Rau et al., 2015) resulting in almost
445 complete damping by 1 m bgl. Furthermore, the daily temperature range within the cave
446 itself is just 0.08-1.53 °C, primarily due to air exchange moderated by conductive
447 equilibrium with the cave walls. The variation of water viscosity (which is inversely
448 proportional to hydraulic conductivity) is approximately 2 to 3 % per degree in the range
449 10 to 30 °C. Considering that the amplitude of a 1 cpd drip rate fluctuation can be as much
450 as 75 % of the maximum drip rate, the greatest anticipated change in hydraulic conductivity,
451 and therefore the drip rate (proportional to the hydraulic conductivity by Darcy's law), on a
452 daily cycle, is likely to be 2-3 orders of magnitude lower than the observed variation in drip
453 rate on a daily basis. We therefore conclude that the daily fluctuations in drip rate are
454 unlikely to be caused by variations in hydraulic conductivity due to changes in viscosity of
455 water.

456

457 **4.2.5. Solar driven daily cycles of (phreatophytic) evapotranspiration**

458 The timing of the daily drip rate signal appears to be associated with the difference in
459 maximum and minimum surface temperature. In the examples examined in more depth in
460 Fig. 4a-b, when the difference between the maximum and minimum temperature was high
461 (17- 22 °C) and the evapotranspiration was relatively high (mean 3.6 mm/day) the 1cpd
462 signal was continuous. Conversely, when the temperature difference was small (4.5-12.7 °C)
463 and the potential evapotranspiration was relatively lower (mean 2.2 mm/day), the 1 cpd
464 signal dissolved into chaos.

465 During periods when there are 1 cpd oscillations in drip rate, there was a relationship
 466 between drip rate and surface temperature on a weekly timescale. The best example, in Fig.
 467 6 where $\tau = -0.21$ (significant at 95%) for a 2-day average air temperature and drip rate at G1
 468 from 01-19/02/2014. We have demonstrated above that it cannot be air temperature
 469 driving the signal through either atmospheric tides or water viscosity changes. However, the
 470 relationship between surface temperature variability and 1 cpd drip rate oscillations could
 471 be explained if the association with diurnal temperature variability is due to variations in
 472 solar radiation received at the surface, as solar radiation and air temperature influence
 473 transpiration (among other factors). We hypothesise that firstly, tree water use was
 474 driving the intermittent daily oscillations in drip discharge demonstrated by the relationship
 475 between daily to weekly variations in surface air temperature and drip discharge and
 476 secondly, the sporadic nature of the oscillations was driven by complexities in the karst
 477 architecture. It has been widely accepted that tree water use causes fluctuations of the
 478 water table (Gribovszki et al 2010; Acworth et al 2015). However, this is the first study that
 479 demonstrates diurnal fluctuation in cave drip rates most likely driven by tree water use.



480

481 Figure 6: Surface air temperature, evapotranspiration and drip discharge rate with the
 482 corresponding daily moving average for site G1 01/02/2014-19/02/2014.

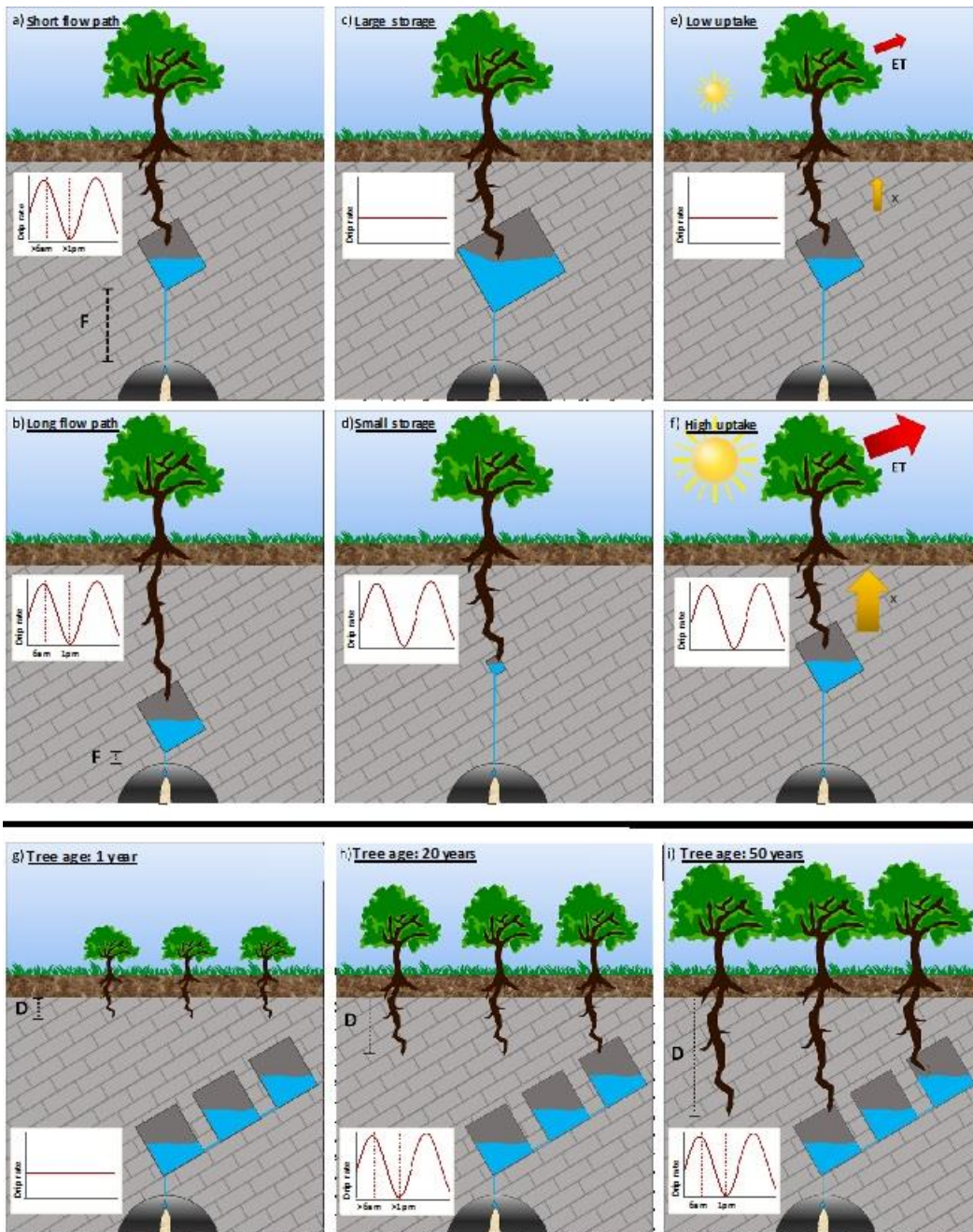
483

484 The area above the cave and in the small uphill catchment is dominated by *E. pauciflora* and
485 *E. stelullata* (Fig. 1). Eucalypt species have a bimodal root system with shallow lateral roots
486 and vertically descending roots which penetrate into the profile to depths of up to 18 m,
487 with depth depending on soil characteristics and the degree to which the bedrock is
488 fractured and conduits developed (Crombie, 1992; Farrington et al., 1996). Hence, these
489 trees have the mechanism to abstract water from karst stores at depth which supports our
490 theory that tree water use causes daily oscillations in cave drip rate.

491 Tree water use from deep roots occurs when the upper layers are too dry and have a lower
492 water potential than the soil water at deeper levels (Dawson and Pate, 1996; Zapater et al.,
493 2011). Maximum tree water use by the roots is therefore expected in the afternoon during
494 the period of maximum solar radiation, possibly lagged due to the time taken to
495 hydraulically lift the water. Conversely, minimum tree water use is expected at the end of
496 night around 6am. Burgess et al (2001) measured sap flow in Eucalypt tap roots, finding tap
497 root sap flow peaked around 1 pm and negative sap flow values indicated reverse
498 (acropetal) flow between 7pm- 7am. In consideration of this, drip water that comes from
499 fractures and stores which contain tree roots would be expected to have a minimum drip
500 discharge in the afternoon and maximum around sunrise. In reality, we observe more
501 complex daily drip oscillations, with peak drip rate occurring at different times of the day
502 and different times of the year. This is to be expected from a karstified system with flow
503 routed through a varied and complex fractured network. Different scenarios for daily
504 oscillations in a karst system will be discussed in detail below.

505 **4.2.5.1 Scenarios for solar driven daily cycles of phreatophytic evapotranspiration**

506



507

508 Figure 7: A conceptual representation of tree water use from karst stores under different
 509 circumstances. a) and b) show different karst store-drip site flow path lengths (F) as the tree
 510 roots access karst stores at different depths; c) and d) show tree roots accessing karst stores
 511 with different volumes; the influence of annual insolation on evapotranspiration (ET) and
 512 root water uptake (x) during winter and summer is shown in e) and f) respectively. Finally,
 513 the increase in rooting depth (D) and access to deeper karst stores over time in years is
 514 explored in subfigures g-i.

515 The depth of a store could affect the timing of daily drip rate oscillations due to the delay in
 516 tree water transport. For example, consider the hypothetical, identical trees with roots
 517 intercepting identical karst stores or fractures at *different* depths in Fig. 7a and 7b. There is

518 likely to be a greater lag in drip response in Fig. 7a than Fig. 7b because of the longer flow
519 path-length (F) from the tree root to the cave drip site. Given that eucalypt tap roots can
520 penetrate to depths ranging from 5-20 m with tap root length depending on the depth of
521 accessible water (Carbon et al., 1980; Dawson and Pate, 1996) and the drip sites at Glory
522 Hole Cave are located 30-50 m below the surface, we can speculate that the minimum flow
523 path length between a taproot accessing the karst store and the drip site below could vary
524 from 10-45 m. In reality, it is difficult to calculate exact flow path length because of the
525 prevalence of lateral flow in heavily karstified systems. This has been demonstrated by
526 Markowska et al (2016) in a study where water spiked with a tracer was used to irrigate the
527 surface above a cave resulting in a response at discharge sites located 7 m laterally from the
528 irrigation location. Across all sites, lag time between maximum air temperature and
529 minimum drip rate ranged from 0.25- 24 hours (Table 2). We can hypothesise that those
530 sites with a shorter lag time have a shorter path length from tree root accessed store to
531 cave discharge site than the other drip sites. For example, the lag time for site G1 ranges
532 from 11.25- 12.75 hours whereas site G10 ranges from 0.5- 3 hours. This process could also
533 explain the large variation in lag time within a particular site, for example at G6 the lag time
534 was 21 hours in May 2014 and decreased to 7 hours in August 2014 (Table 2). We
535 hypothesise that the change could be due to a shortening of the path length from root
536 accessed store to cave discharge site as the tree grows and increases its rooting depth, thus
537 accessing a deeper water store. Alternatively, this could also be the result of compensation
538 as a shallow water store dries up and a deeper section of the root network is utilised.

539 The size of the karst store, or volume of water within the store, could determine whether
540 the daily oscillation is observable or not. Consider the conceptual Fig. 7c and 7d, where
541 identical trees have roots intercepting different karst stores at the *same* depth. We propose
542 that a daily oscillation will only be observed when the tree water use is a significant part of
543 the total water store so a daily oscillation is more likely to be observed in the smaller store
544 (Fig. 7d) than a store with a larger volume (Fig. 7c). The influence of store volume on the
545 presence of daily oscillations could also explain why the phenomenon is not observed at
546 M1. In section 3.1 we discuss how the low, consistent drip rate at M1 responds to seasonal
547 drying but does not respond to individual rainfall events. We propose that this site is fed by
548 a store large enough to assimilate individual rainfall events and the same line of reasoning
549 could explain the lack of response to tree water use, the volume of water extracted by tree
550 roots is insignificant in relation to the large volume of water in the store. Conversely, we can
551 hypothesise that G6 has a small store volume that is more sensitive to water uptake by tree
552 roots, which is why we see the minimum drip rate occurring 0.25-7 hours before peak air
553 temperature (Table 2). Furthermore, this scenario is supported by the fact that, generally,
554 the daily oscillations are not exhibited during periods of high rainfall, and consequently high
555 drip discharge, as the tree use signal is more likely to be a smaller fraction of the total water
556 volume. Sites G1, G3 M2 and M4 have high seasonal discharge rates during June-September
557 as indicated by the multiple hydrograph peaks for the corresponding sites in Fig. 3. There

558 are no daily oscillations during these periods of peak discharge at any of these sites. Daily
559 oscillations coincide with the receding limb of the peak at sites M4 (July and September
560 2013) and M4 (September 2013) as the drip rate decreases. The non-observance of daily
561 oscillations during periods of high rainfall could also be attributed to the redistribution of
562 water by the roots from the saturated soil to the unsaturated subsurface (Burgess et al.,
563 2001).

564 Tree water use responds to annual variation in insolation. Consider Fig. 7e and Fig. 7f where
565 one tree root intercepts the same karst store over the course of a year. During winter (Fig
566 7e), there is less insolation than the summer (Fig 7f) therefore the rate of
567 evapotranspiration is lower. This means that in winter the hydraulic lift (i) is low or negative
568 and daily oscillations in drip discharge could be dampened or absent. Our analysis reveals
569 that only 2 out of 41 periods of 1 cpd oscillation occur during winter months June-August
570 (G6 between 14-24/8/13 and M2 between 8-13/7/2013). However, our analysis also
571 revealed that season did not explain a significant amount of variance in lag time, thus
572 suggesting that more variables, such as karst architecture, are affecting the timing of drip
573 rate oscillations.

574 In reality, there are multiple trees of different ages above the cave, further complicating the
575 flow variability. Figure 7g-i presents a conceptual representation of tree tap root length
576 increasing (L) as the tree grows and accesses deeper karst stores over 1-50 year timescale.
577 This response to annual insolation and the interaction of multiple trees of varying ages could
578 explain why daily oscillations at an individual drip site occur one year and not the next, for
579 example at M10 there is a 1 cpd in December 2012 however, this oscillation does not occur
580 at the same time in 2013 or 2014. The mechanism in Fig. 7i could also explain why 2 cpd
581 signals are also observed, whereby multiple tree roots are accessing interconnected water
582 stores at different depths resulting in two separate cycles with differing lag times. The
583 occurrence of 2 cpd signals in drip rate could also be related to signal processing where if
584 the signal is not strictly sinusoidal there may be harmonics in the spectrum. This finding and
585 the interpretation is an area for further research.

586 **4.6 Implications for karst architecture and climate proxy modelling research**

587 Karst architecture controls flow regimes and drip discharge rates of water infiltrating into
588 caves (e.g., Markowska et al., 2015). Flow rate influences speleothem climate proxies, such
589 as the $\delta^{18}\text{O}$ and concentration of solutes in drip water, through the dilution and mixing of
590 percolation waters prior to reaching the cave. It is important to distinguish between the
591 influence of karst architecture and climate-driven processes, such as drought, on discharge
592 so that paleoclimate proxy records from associated speleothems can be appropriately
593 constrained. This study has increased our understanding of karst architecture, information
594 which can be utilised in proxy-system models or forward models, approaches that are
595 increasingly used to understand cave drip rate variability and to model speleothem proxies
596 such as $\delta^{18}\text{O}$ (Bradley et al., 2010; Cuthbert et al., 2014a). Additionally, we propose that an

597 important part of any protocol for inferring karst architecture is 1) the incorporation of cave
598 drip rate monitoring with a minimum 15 min interval at multiple discharge sites for at least a
599 year and 2) the systematic investigation of daily, weekly and monthly timescales using
600 frequency analysis capable of showing frequency-time changes, such as the synchrosqueeze
601 transform (Daubechies et al., 2011) to infer karst flow processes and their relative
602 importance. This study clearly demonstrates the potential for vegetation to impact karst
603 water recharge making this research relevant to karst modelling and karst water resources
604 assessment. Currently, there are no approaches that consider the impacts of vegetation on
605 recharge dynamics in process-based karst models (Hartmann et al., 2014b, 2015) or in
606 empirical recharge estimation approaches (Allocca et al., 2014; Andreo et al., 2006).

607 This is the first indirect volumetric observation of tree water use in cave drip water. This
608 supports a growing number of studies examining the impact of trees on karst processes and
609 paleoclimate proxies. For example, tree root respiration provides a source of CO₂ for the
610 dissolution of limestone that is additional to that from soil and vadose zone microbial
611 respiration. Coleborn et al (2016) found that vegetation regeneration determined post-fire
612 soil CO₂ in a study investigating post-fire impacts on karst processes. Direct observations of
613 tree water use within the karst unsaturated zone implies the presence of root respiration, a
614 process which in turn affects drip water and speleothem ¹⁴C and δ¹³C composition (Fairchild
615 and Baker, 2012; Meyer et al., 2014; Noronha et al., 2015). Trees have been demonstrated
616 to have long-term effects on cave drip-water solute concentrations. Treble et al. (2015,
617 submitted) demonstrate long-term trends in drip water calcium and trace element
618 concentration, which they attribute to increasing solute concentration due to forest
619 regrowth and increased post-fire tree water use. Baldini et al (2005) infer an effect on
620 speleothem δ¹⁸O due to secondary forest regrowth after mining and Wong and Banner
621 (2010) found clearing surface vegetation changed drip water Mg/Ca and Sr/Ca. The findings
622 and suggested protocol in this study will inform the selection of speleothem specimens for
623 further research into the impact of tree water use on speleothem paleoclimate proxies.

624 **5. Conclusions**

625

626 We demonstrated a novel method of analysing recurring patterns in cave water drip rate
627 using the wavelet synchrosqueezed transform (WSST). Our analysis revealed daily and sub-
628 daily oscillations with variable temporal and spatial signatures. We tested competing
629 hypotheses for causes of daily oscillations using drip rate, barometric and temperature data.
630 The only hypothesis which all the data and hydrologic theory were consistent with, was that
631 daily fluctuations in drip rate were driven by tree water use. We proposed that the
632 complexity of flow pathways in the karst system accounted for the spatial and temporal
633 variation in the daily fluctuations of drip rates. This was explored in detail using conceptual
634 models. The results have wider implications for karst research including providing a new
635 protocol for inferring karst architecture, informing selection of speleothem specimens for

636 tree water use paleoclimate studies and highlighting the importance of vegetation dynamics
637 on karst recharge.

638

639 **Author contribution**

640 KC, MOC, GCR and AB wrote the manuscript, discussed the results and implications and
641 commented on the manuscript at all stages. KC, AB and ON collected data. GCR performed
642 the WSST analysis and generated the WSST and CWT figures. GCR and ON created the
643 location map. KC generated other graphs and conceptual figures.

644 **Acknowledgements**

645 We acknowledge that Katie Coleborn was supported the Australian Research Council
646 (LP130100177). Mark Cuthbert was supported by Marie Curie Research Fellowship funding
647 from the European Community's Seventh Framework Programme [FP7/2007-2013] under
648 grant agreement n.299091. We would also like to thank Stuart Hankin for allowing us access
649 to the weather station data and the National Parks and Wildlife Service staff at Yarrangobilly
650 Caves. Solar exposure data derived from satellite imagery processed by the Bureau of
651 Meteorology from the Geostationary Meteorological Satellite and MTSAT series operated by
652 Japan Meteorological Agency and from GOES-9 operated by the National Oceanographic &
653 Atmospheric Administration (NOAA) for the Japan Meteorological Agency. We would also
654 like to acknowledge the use of equipment funded by the Australian Government National
655 Collaborative Research Infrastructure Strategy (NCRIS).

656 **References**

- 657 Acworth, R. I., Rau, G. C., McCallum, A. M., Andersen, M. S. and Cuthbert, M. O.:
658 Understanding connected surface-water/groundwater systems using Fourier analysis of
659 daily and sub-daily head fluctuations, *Hydrogeol. J.*, 23(1), 143–159, doi:10.1007/s10040-
660 014-1182-5, 2015.
- 661 Adamson, L. and Loudon, A.: Wagga Geological Sheet, SI/55-15, 1st edition, 1:250000, 1966.
- 662 Allocca, V., Manna, F. and De Vita, P.: Estimating annual groundwater recharge coefficient
663 for karst aquifers of the southern Apennines (Italy), *Hydrol. Earth Syst. Sci.*, 18(2), 803–817,
664 doi:10.5194/hess-18-803-2014, 2014.
- 665 Andreo, B., Vias, J., Duran, J. J. and Jimenez, P.: Methodology for groundwater recharge
666 assessment in carbonate aquifers: application to pilot sites in southern Spain, *Hydrogeol. J.*,
667 16, 911–925, 2006.
- 668 Arbel, Y., Greenbaum, N., Lange, J. and Inbar, M.: Infiltration processes and flow rates in
669 developed karst vadose zone using tracers in cave drips, *Earth Surf. Process. Landforms*,
670 35(14), 1682–1693, doi:10.1002/esp.2010, 2010.
- 671 Auger, F. and Flandrin, P.: Improving the readability of time-frequency and time-scale

672 representations by the reassignment method, *IEEE Trans. Signal Process.*, 43(5), 1068–1089,
673 doi:10.1109/78.382394, 1995.

674 Baker, a., Bradley, C., Phipps, S. J., Fischer, M., Fairchild, I. J., Fuller, L., Spötl, C. and Azcurra,
675 C.: Millennial-length forward models and pseudoproxies of stalagmite $\delta^{18}\text{O}$: an example
676 from NW Scotland, *Clim. Past*, 8(4), 1153–1167, doi:10.5194/cp-8-1153-2012, 2012.

677 Baker, A. and Brunsdon, C.: Non-linearities in drip water hydrology: an example from Stump
678 Cross Caverns, Yorkshire, *J. Hydrol.*, 277(3-4), 151–163, doi:10.1016/S0022-1694(03)00063-
679 5, 2003.

680 Baldini, J. U. L., McDermott, F., Baker, a, Baldini, L. M., Matthey, D. P. and Railsback, L. B.:
681 Biomass effects on stalagmite growth and isotope ratios: A 20th century analogue from
682 Wiltshire, England, *Earth Planet. Sci. Lett.*, 240(2), 486–494, doi:10.1016/j.epsl.2005.09.022,
683 2005.

684 Baldini, J. U. L., McDermott, F., Baldini, L. M., Ottley, C. J., Linge, K. L., Clipson, N. and Jarvis,
685 K. E.: Identifying short-term and seasonal trends in cave drip water trace element
686 concentrations based on a daily-scale automatically collected drip water dataset, *Chem.*
687 *Geol.*, 330-331, 1–16, doi:10.1016/j.chemgeo.2012.08.009, 2012.

688 Bradley, C., Baker, A., Jex, C. N. and Leng, M. J.: Hydrological uncertainties in the modelling
689 of cave drip-water $\delta^{18}\text{O}$ and the implications for stalagmite palaeoclimate reconstructions,
690 *Quat. Sci. Rev.*, 29(17-18), 2201–2214, doi:10.1016/j.quascirev.2010.05.017, 2010.

691 Burgess, S. S. O., Adams, M. a., Turner, N. C., White, D. a. and Ong, C. K.: Tree roots:
692 Conduits for deep recharge of soil water, *Oecologia*, 126(2), 158–165,
693 doi:10.1007/s004420000501, 2001.

694 Carbon, B. A., Bartle, G. A., Murray, A. M. and Macpherson, D. K.: The distribution of root
695 length, and the limits to flow of soil water to roots in a dry sclerophyll forest, *For. Sci.*, 26(4),
696 656–664, 1980.

697 Collister, C. and Matthey, D.: Controls on water drop volume at speleothem drip sites: An
698 experimental study, *J. Hydrol.*, 358, 259–267, doi:10.1016/j.jhydrol.2008.06.008, 2008.

699 Crombie, D. S.: Root depth, leaf area and daytime water relations of Jarrah (*Eucalyptus*
700 *marginata*) forest overstorey and understorey during summer drought, *Aust. J. Bot.*,
701 40(1988), 113–22, doi:10.1071/BT9920113, 1992.

702 Cuthbert, M., Baker, A., Jex, C., Graham, P., Treble, P., Andersen, M. and Acworth, I.: Drip
703 water isotopes in semi-arid karst: Implications for speleothem paleoclimatology, *Earth*
704 *Planet. Sci. Lett.*, 395, 194–204, doi:10.1016/j.epsl.2014.03.034, 2014a.

705 Cuthbert, M. O., Rau, G. C., Andersen, M. S., Roshan, H., Rutledge, H., Marjo, C. E.,
706 Markowska, M., Jex, C. N., Graham, P. W., Mariethoz, G., Acworth, R. I. and Baker, a:
707 Evaporative cooling of speleothem drip water., *Sci. Rep.*, 4, 5162, doi:10.1038/srep05162,
708 2014b.

709 Daubechies, I., Lu, J. and Wu, H. T.: Synchrosqueezed wavelet transforms: An empirical
710 mode decomposition-like tool, *Appl. Comput. Harmon. Anal.*, 30(2), 243–261,

711 doi:10.1016/j.acha.2010.08.002, 2011.

712 Dawson, T. E. and Pate, J. S.: Seasonal water uptake and movement in root systems of
713 Australian phraeatophytic plants of dimorphic root morphology: a stable isotope
714 investigation, *Oecologia*, 107(1), 13–20, doi:10.1007/BF00582230, 1996.

715 Fairchild, I. J. and Baker, A.: *Speleothem Science: From Process to Past Environments*, 1st
716 ed., Wiley-Blackwell., 2012.

717 Fairchild, I. J., Borsato, A., Tooth, A. F., Frisia, S., Hawkesworth, C. J., Huang, Y. and
718 Mcdermott, F.: Controls on trace element δ Sr – Mg / compositions of carbonate cave
719 waters : implications for speleothem climatic records, 2000.

720 Farrington, P., Turner, J. and Gailitis, V.: *Eucalyptus marginata*, *Trees*, 11, 9–15, 1996.

721 Ford D. and P. D. Williams (1994) *Karst Hydrogeology and Geomorphology*, Wiley,
722 Chichester.

723 Genty, D. and Deflandre, G.: Drip flow variations under a stalactite of the Pere Noel cave
724 (Belgium). Evidence of seasonal variations and air pressure constraints, *J. Hydrol.*, 211(1-4),
725 208–232, doi:10.1016/S0022-1694(98)00235-2, 1998.

726 Gribovski, Z., Szilágyi, J. and Kalicz, P.: Diurnal fluctuations in shallow groundwater levels
727 and streamflow rates and their interpretation - A review, *J. Hydrol.*, 385(1-4), 371–383,
728 doi:10.1016/j.jhydrol.2010.02.001, 2010.

729 Hartmann, a, Goldscheider, N., Wagener, T., Lange, J. and Weiler, M.: Karst water resources
730 in a changing world: Approaches, of hydrological modeling, *Rev. Geophys.*, (1), 1–25,
731 doi:10.1002/2013RG000443.Received, 2014a.

732 Hartmann, A., Mudarra, M., Andreo, B., Marin, A., Wagener, T. and Lange, J.: Modelling
733 spatiotemporal impacts of hydroclimatic extremes on groundwater recharge at a
734 Mediterranean karst aquifer, *Water Resour. Res.*, 50, 6507–6521,
735 doi:10.1002/2014WR015685.Received, 2014b.

736 Hartmann, A., Gleeson, T., Rosolem, R., Pianosi, F., Wada, Y. and Wagener, T.: A large-scale
737 simulation model to assess karstic groundwater recharge over Europe and the
738 Mediterranean, *Geosci. Model Dev.*, 8(6), 1729–1746, doi:10.5194/gmd-8-1729-2015, 2015.

739 Hu, C., Henderson, G. M., Huang, J., Chen, Z. and Johnson, K. R.: Report of a three-year
740 monitoring programme at Heshang Cave, Central China, *Int. J. Speleol.*, 37(October), 143–
741 151, doi:10.5038/1827-806X.37.3.1, 2008.

742 Jex, C. N., Mariethoz, G., Baker, A., Graham, P., Andersen, M. S., Acworth, I., Edwards, N.
743 and Azcurra, C.: Spatially dense drip hydrological monitoring and infiltration behaviour at
744 the Wellington Caves, South East Australia, *Int. J. Speleol.*, 41(2), 283–296, 2012.

745 Lange, J., Arbel, Y., Grodek, T. and Greenbaum, N.: Water percolation process studies in a
746 Mediterranean karst area, *Hydrol. Process.*, 24(13), 1866–1879, doi:10.1002/hyp.7624,
747 2010.

748 Mahmud, K., Mariethoz, G., Baker, a., Treble, P. C., Markowska, M. and McGuire, E.:

- 749 Estimation of deep infiltration in unsaturated limestone environments using cave LiDAR and
750 drip count data, *Hydrol. Earth Syst. Sci. Discuss.*, 12(9), 8891–8925, doi:10.5194/hessd-12-
751 8891-2015, 2015.
- 752 Mariethoz, G., Baker, A., Sivakumar, B., Hartland, A. and Graham, P.: Chaos and irregularity
753 in karst percolation, *Geophys. Res. Lett.*, 39(23), n/a–n/a, doi:10.1029/2012GL054270, 2012.
- 754 Markowska, M., Baker, A., Treble, P. C., Andersen, M. S., Hankin, S., Jex, C. N., Tadros, C. V.
755 and Roach, R.: Unsaturated zone hydrology and cave drip discharge water response:
756 Implications for speleothem paleoclimate record variability, *J. Hydrol.*,
757 doi:10.1016/j.jhydrol.2014.12.044, 2015.
- 758 McDonald, J.: The 2002–2003 El Niño recorded in Australian cave drip waters: Implications
759 for reconstructing rainfall histories using stalagmites, *Geophys. Res. Lett.*, 31(22),
760 doi:10.1029/2004GL020859, 2004.
- 761 McDonald, J. and Drysdale, R.: Hydrology of cave drip waters at varying bedrock depths
762 from a karst system in southeastern Australia, *Hydrol. Process.*, 1748(March), 1737–1748,
763 doi:10.1002/hyp, 2007.
- 764 Merritt, M. L.: Estimating Hydraulic Properties of the Floridan Aquifer System by Analysis of
765 Effects , *Collier and Hendry Counties , Florida, Secretary*, 70, 2004.
- 766 Meyer, K. W., Feng, W., Breecker, D. O., Banner, J. L. and Guilfoyle, A.: Interpretation of
767 speleothem calcite $\delta^{13}\text{C}$ variations: Evidence from monitoring soil CO_2 , drip water, and
768 modern speleothem calcite in central Texas, *Geochim. Cosmochim. Acta*, 142, 281–298,
769 doi:10.1016/j.gca.2014.07.027, 2014.
- 770 Noronha, A. L., Johnson, K. R., Southon, J. R., Hu, C., Ruan, J. and McCabe-Glynn, S.:
771 Radiocarbon evidence for decomposition of aged organic matter in the vadose zone as the
772 main source of speleothem carbon, *Quat. Sci. Rev.*, 127, 37–47,
773 doi:10.1016/j.quascirev.2015.05.021, 2015.
- 774 Peel, M. C., Finlayson, B. L. and McMahon, T. a: Updated world map of the Köppen-Geiger
775 climate classification, *Hydrol. Earth Syst. Sci. Discuss.*, 4, pp. 439–473, doi:10.5194/hess-11-
776 1633-2007, 2007.
- 777 Proctor, C. J., Baker, a., Barnes, W. L. and Gilmour, M. a.: A thousand year speleothem
778 proxy record of North Atlantic climate from Scotland, *Clim. Dyn.*, 16(10-11), 815–820,
779 doi:10.1007/s003820000077, 2000.
- 780 Rau, G. C., Cuthbert, M. O., Andersen, M. S., Baker, A., Rutledge, H., Markowska, M., Roshan,
781 H., Marjo, C. E., Graham, P. W. and Acworth, R. I.: Controls on cave drip water temperature
782 and implications for speleothem-based paleoclimate reconstructions, *Quat. Sci. Rev.*, 127,
783 1–18, doi:10.1016/j.quascirev.2015.03.026, 2015.
- 784 Rutledge, H., Baker, A., Marjo, C. E., Andersen, M. S., Graham, P. W., Cuthbert, M. O., Rau, G.
785 C., Roshan, H., Markowska, M., Mariethoz, G. and Jex, C. N.: Dripwater organic matter and
786 trace element geochemistry in a semi-arid karst environment: Implications for speleothem
787 paleoclimatology, *Geochim. Cosmochim. Acta*, 135, 217–230,
788 doi:10.1016/j.gca.2014.03.036, 2014.

- 789 Sheffer, N. a., Cohen, M., Morin, E., Grodek, T., Gimburg, A., Magal, E., Gvirtzman, H., Nied,
790 M., Isele, D. and Frumkin, A.: Integrated cave drip monitoring for epikarst recharge
791 estimation in a dry Mediterranean area, Sif Cave, Israel, *Hydrol. Process.*, 25(18), 2837–
792 2845, doi:10.1002/hyp.8046, 2011.
- 793 Sondag, F., Van Ruymbeke, M., Soubiès, F., Santos, R., Somerhausen, A., Seidel, A. and
794 Boggiani, P.: Monitoring present day climatic conditions in tropical caves using an
795 Environmental Data Acquisition System (EDAS), *J. Hydrol.*, 273(1-4), 103–118,
796 doi:10.1016/S0022-1694(02)00362-1, 2003.
- 797 Spate, A.: *Karst Values*, Hurstville., 2002.
- 798 Stern, H., Hoedt, G. de and Ernst, J.: Objective classification of Australian Climates, *Bur.*
799 *Meteorol.* [online] Available from:
800 http://www.bom.gov.au/climate/environ/other/koppen_explain.shtml (Accessed 15
801 October 2013), 2012.
- 802 Thakur, G., Brevdo, E., Fučkar, N. S. and Wu, H. T.: The Synchrosqueezing algorithm for time-
803 varying spectral analysis: Robustness properties and new paleoclimate applications, *Signal*
804 *Processing*, 93(5), 1079–1094, doi:10.1016/j.sigpro.2012.11.029, 2013.
- 805 Tooth, A. F. and Fairchild, I. J.: Soil and karst aquifer hydrological controls on the
806 geochemical evolution of speleothem-forming drip waters, Crag Cave, southwest Ireland, *J.*
807 *Hydrol.*, 273(1-4), 51–68, doi:10.1016/S0022-1694(02)00349-9, 2003.
- 808 Torrence, C., Compo, G. P.: A Practical Guide to Wavelet Analysis, *Bull. Amer. Meteor. Soc.*,
809 79, 61–78, doi: 10.1175/1520-0477(1998)079<0061:APGTWA>2.0.CO;2.
- 810 Treble, P., Markowska, M., Tadros, C., Jex, C., Coleborn, K., Dredge, J., Baker, A., Roach, R.
811 and Spate, A.: Reconstructing past environmental change at Yarrangobilly Caves, pp. 83–88.,
812 2013a.
- 813 Treble, P. C., Bradley, C., Wood, A., Baker, A., Jex, C. N., Fairchild, I. J., Gagan, M. K., Cowley,
814 J. and Azcurra, C.: An isotopic and modelling study of flow paths and storage in Quaternary
815 calcarenite, SW Australia: implications for speleothem paleoclimate records, *Quat. Sci. Rev.*,
816 64, 90–103, doi:10.1016/j.quascirev.2012.12.015, 2013b.
- 817 Treble, P. C., Fairchild, I. J., Griffiths, A., Baker, A., Meredith, K. T., Wood, A. and McGuire, E.:
818 Impacts of cave air ventilation and in-cave prior calcite precipitation on Golgotha Cave
819 dripwater chemistry, southwest Australia, *Quat. Sci. Rev.*, 127,
820 doi:10.1016/j.quascirev.2015.06.001, 2015.
- 821 Treble, P. C., Fairchild, I. J., Baker, A., Meredith, K. M., Andersen, M. S., Salmon, S. U.,
822 Bradley, C., Wynn, P. M., Hankin, S., Wood, A. and McGuire, E.: Roles of bioproductivity,
823 transpiration and fire in an eight-year record of cave dripwater chemistry from a forested
824 catchment, southwest Australia, 2016.
- 825 Tremaine, D. M. and Froelich, P. N.: Speleothem trace element signatures: A hydrologic
826 geochemical study of modern cave dripwaters and farmed calcite, *Geochim. Cosmochim.*
827 *Acta*, 121, 522–545, doi:10.1016/j.gca.2013.07.026, 2013.

- 828 Webb, M., Dredge, J., Barker, P. A., Müller, W., Jex, C., Desmarchelier, J., Hellstrom, J. and
829 Wynn, P. M.: Quaternary climatic instability in south-east Australia from a multi-proxy
830 speleothem record, *J. Quat. Sci.*, 29(6), 589–596, doi:10.1002/jqs.2734, 2014.
- 831 Wong, C. and Banner, J. L.: Response of cave air CO₂ and drip water to brush clearing in
832 central Texas: Implications for recharge and soil CO₂ dynamics, *J. Geophys. Res.*, 115,
833 doi:10.1029/2010JG001301, 2010.
- 834 Worboys, G.: Kosciusko National Park Geology and Geomorphology, National Parks and
835 Wildlife Services, Sydney., 1982.
- 836 Zapater, M., Hossann, C., Bréda, N., Bréchet, C., Bonal, D. and Granier, A.: Evidence of
837 hydraulic lift in a young beech and oak mixed forest using ¹⁸O soil water
838 labelling, *Trees - Struct. Funct.*, 25(5), 885–894, doi:10.1007/s00468-011-0563-9, 2011.
- 839